CHAPTER IV
RESULTS AND DISCUSSION

4.1 Characterization Results

4.1.1 TG Analysis

The TG curve was used to study the thermal decomposition behavior of the synthesized dried TiO_2 gel and to obtain its suitable calcination temperature. Figure 4.1 shows the TG curve of the dried TiO_2 gel. The TG result reveals that the calcination temperature of approximately 425 °C was sufficient for both the complete LAHC surfactant removal and the photocatalyst crystallization. It should be noted from experimental observation that at the calcination temperature below 400 °C, the obtained TiO_2 film had yellow color, indicating that the organic molecules used during the synthesis step could not be completely removed during the calcination step. Therefore, the calcination temperature in the range of 400 to 500 °C was used to investigate its effect on the physicochemical properties and consequent photocatalytic AB dye degradation activity of the immobilized TiO_2 synthesized by the sol-gel method. It should also be noted that the glass plate used for TiO_2 immobilization could not withstand a temperature higher than 500 °C.

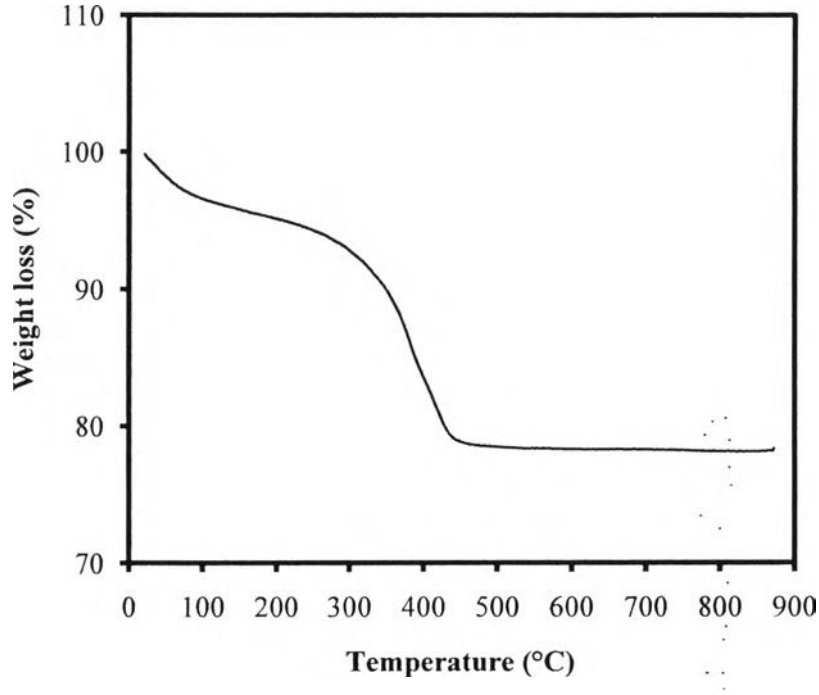

Figure 4.1 TG curve of the as-synthesized dried TiO_2 gel.

4.1.2 N_2 Adsorption-Desorption Analysis

In order to verify the mesoporosity of the photocatalyst samples, N_2 adsorption-desorption analysis is very powerful technique normally used. The shape of the isotherms exhibits the characteristic behavior of the structure of powder, which is composed of an assembly of particles with uniform pore opening. Figures 4.2 and 4.3 depict the exemplified N_2 adsorption-desorption isotherms and pore size distributions (inset) of the synthesized TiO_2 photocatalyst calcined at 500 °C and 5 wt.% P-25 TiO_2-added synthesized TiO_2 photocatalyst calcined at 400 °C, respectively. The isotherms of all the synthesized photocatalysts exhibited typical IUPAC type IV pattern with H2-type hysteresis loop. The hysteresis loop can be ascribed to the existence of mesoporous structure (mesoporous size between 2 and 50 nm) in the obtained products (Rouquerol *et al.*, 1999). A sharp increase in adsorption volume of N_2 was observed and located in the high relative pressure (P/P_0) range of 0.75-0.95. This sharp increase can be assigned to the capillary condensation, indicating good homogeneity of the samples and fairly small pore size since the P/P_0 position of the inflection point is directly related to the pore dimension (Sreethawong *et al.*, 2005). As illustrated in the inset of Figures 4.2 and 4.3, the pore size

distributions obtained from the desorption branch of the isotherms were quite narrow, implying good quality of the samples.

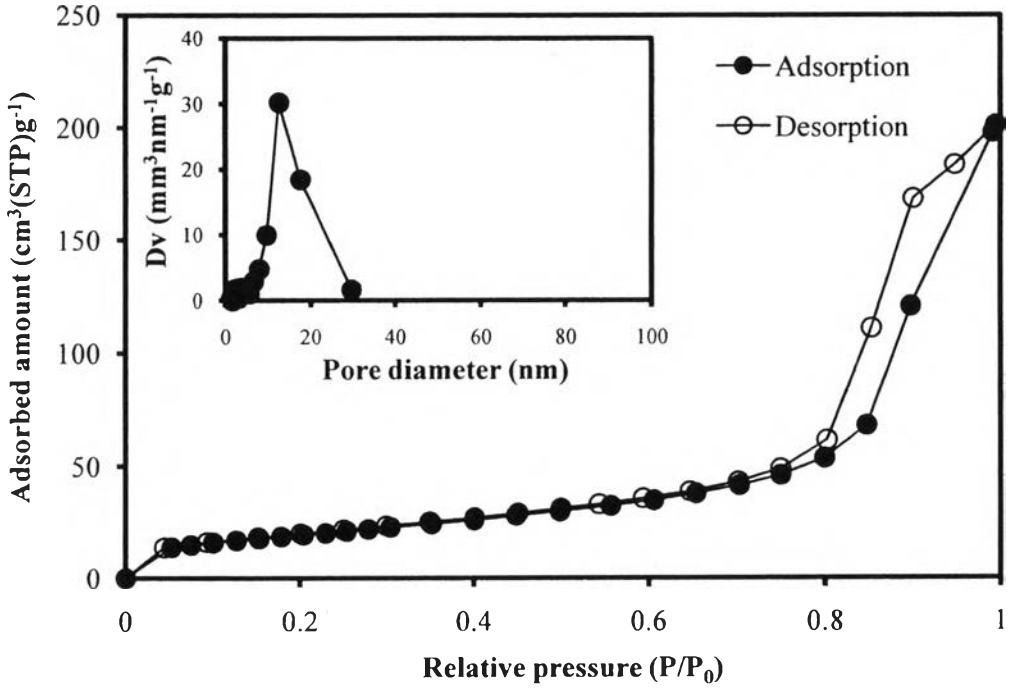

Figure 4.2 N_2 adsorption-desorption isotherms of the synthesized mesoporous-assembled TiO_2 photocatalyst calcined at 500 °C (Inset: Pore size distribution).

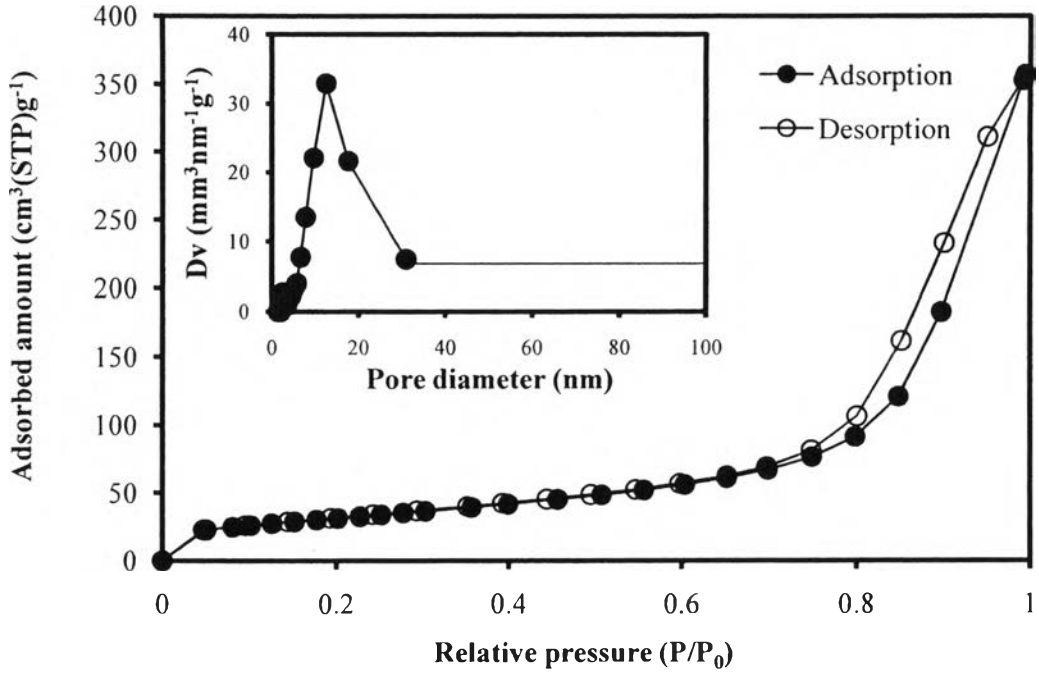

Figure 4.3 N_2 adsorption-desorption isotherms of the 5 wt.% P-25 TiO_2-added synthesized mesoporous-assembled TiO_2 photocatalyst calcined at 400 °C (Inset: Pore size distribution).

The experimental results on textural properties of all investigated photocatalysts, including specific surface area, mean mesopore diameter, and total pore volume, are shown in Table 4.1. For the synthesized mesoporous-assembled TiO_2 photocatalysts without and with 5 wt.% P-25 TiO_2 addition, the increase in calcination temperature caused the decreases in specific surface area and total pore volume and the increase in mean mesopore diameter, as expected. In case of varying P-25 TiO_2 content added to the synthesized mesoporous-assembled TiO_2 photocatalyst calcined at 400 °C, the increase in added P-25 TiO_2 content to 5 wt.% caused the increases in specific surface area and total pore volume, but they adversely decreased with the further increase in added P-25 TiO_2 content up to 7 wt.%, whereas the mean mesopore diameter was not significantly affected.

Table 4.1 N_2 adsorption-desorption results of the synthesized mesoporous-assembled TiO_2 photocatalyst without and with P-25 TiO_2 addition calcined at different temperatures

Photocatalyst	Calcination temperature (°C)	Specific surface area ($m^2 \cdot g^{-1}$)	Mean mesopore diameter (nm)	Total pore volume ($cm^3 \cdot g^{-1}$)
Synthesized TiO_2	400	126.8	9.6	0.363
	450	96.3	12.6	0.354
	500	71.3	12.5	0.306
3 wt.% P-25 TiO_2-added synthesized TiO_2	400	108.2	12.5	0.469
5 wt.% P-25 TiO_2-added synthesized TiO_2		114.2	12.4	0.546
7 wt.% P-25 TiO_2-added synthesized TiO_2		87.2	12.4	0.518
5 wt.% P-25 TiO_2-added synthesized TiO_2	400	114.2	12.4	0.546
	450	78.8	17.5	0.485
	500	58.9	31.5	0.388
P-25 TiO_2	400	47.7	24.3	0.256
	450	47.5	24.3	0.261
	500	44.5	24.3	0.176

4.1.3 UV-Visible Spectroscopy

UV-visible spectroscopy was used to investigate the light absorption capability of the investigated photocatalysts. The UV-visible spectra of the synthesized mesoporous-assembled TiO_2 photocatalyst films coated on glass plate and calcined at different temperatures without and with P-25 TiO_2 addition are shown in Figures 4.4 and 4.5. From Figure 4.4, it can be clearly seen that the absorption band of all the investigated TiO_2 photocatalysts is approximately in the

range of 200–420 nm. The strong absorption band at low wavelength in the spectra indicates the presence of Ti species as tetrahedral Ti^{4+}. This absorption band is generally associated with the electronic excitation of the valence band O2p electron to the conduction band Ti3d level (Fuerte *et al.*, 2002). The energy band gap (E_g, eV) could also be determined by extrapolating the absorption onset of the rising part to x-axis (λ_g, nm) of the UV-visible spectra plots, as exemplified by the dotted lines in Figure 4.4, and calculating by Equation (4.1):

$$E_g = \frac{1240}{\lambda_g} \tag{4.1}$$

The results of absorption onset and band gap energy of the synthesized mesoporous-assembled TiO_2 photocatalysts without and with P-25 TiO_2 addition are summarized in Table 4.2. The absorption onset was observed to be approximately at 375-385 nm for all the synthesized mesoporous-assembled TiO_2 without the P-25 TiO_2 addition, which corresponds to the band gap energy of the anatase TiO_2 of 3.20 eV, whereas the absorbance spectra of the mixture between the synthesized mesoporous-assembled TiO_2 and added P-25 TiO_2 photocatalysts show two absorption onsets at wavelengths of 380-385 and 410-415 nm, where the latter is correlated to the band gap energy of the rutile TiO_2 of 3.02 eV. The presence of two absorption onsets for both anatase and rutile TiO_2 was also clearly seen for the P-25 TiO_2 added-synthesized TiO_2 photocatalyst films with different P-25 TiO_2 contents, as shown in Figure 4.5. This is because the commercial P-25 TiO_2 photocatalyst possesses the mixture of the anatase and rutile TiO_2 phases with about 23 % rutile content (Sreethawong *et al.*, 2005).

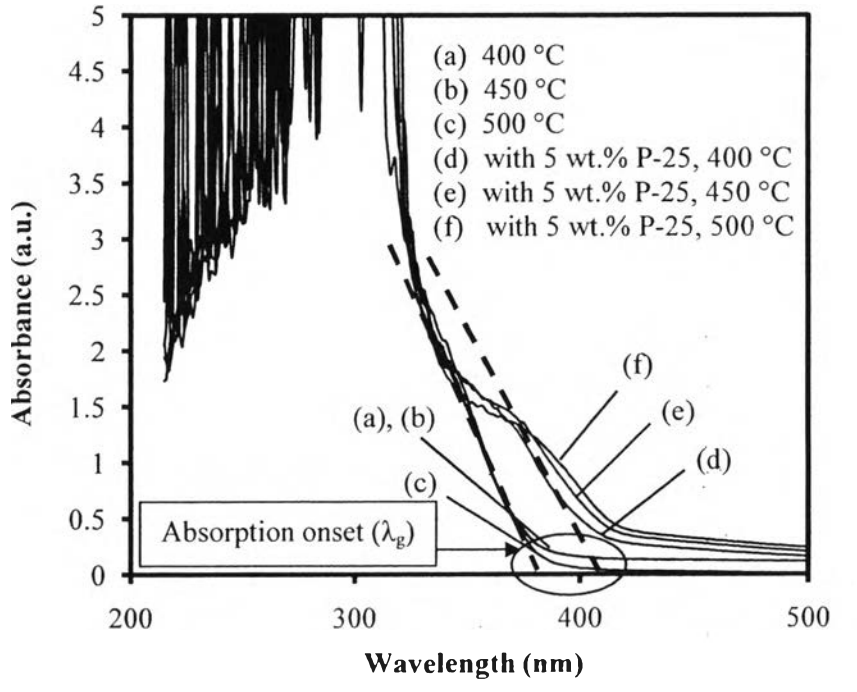

Figure 4.4 UV-visible spectra of the synthesized mesoporous-assembled TiO_2 photocatalyst films coated on glass plate and calcined at different temperatures without and with 5 wt.% P-25 TiO_2 addition.

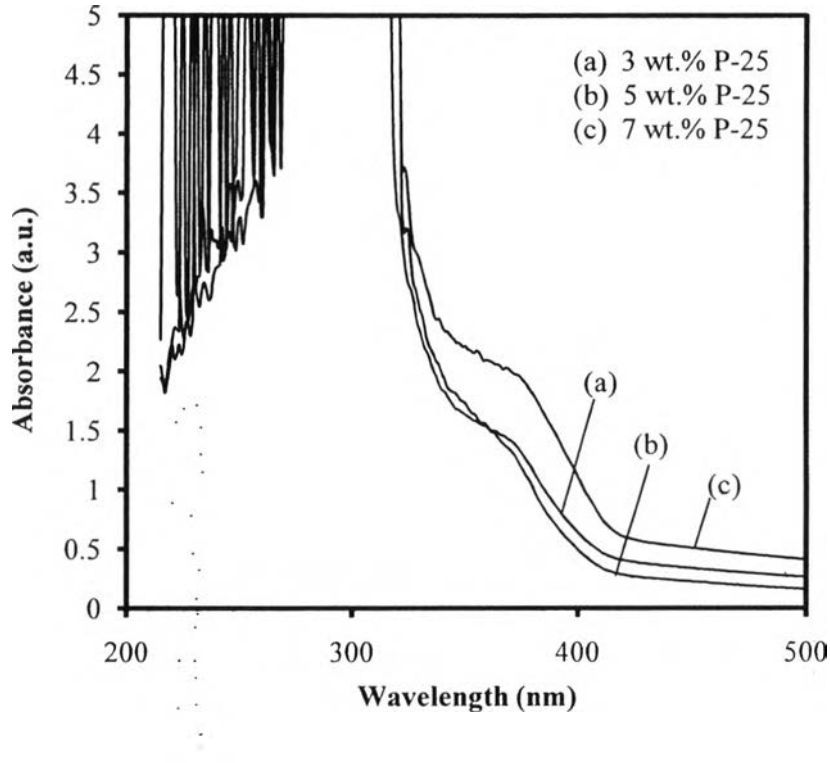

Figure 4.5 UV-visible spectra of the synthesized mesoporous-assembled TiO_2 photocatalyst films coated on glass plate and calcined at 400 °C with P-25 TiO_2 addition at different contents.

Table 4.2 Absorption onset wavelength and band gap energy results of the synthesized mesoporous-assembled TiO_2 photocatalysts coated on glass plate without and with P-25 TiO_2 addition and calcined at different temperatures

Photocatalyst	Calcination temperature (°C)	Absorption onset wavelength, λ_g (nm)	Band gap energy (eV)
Synthesized TiO_2	400	375	3.31
	450	380	3.26
	500	385	3.22
3 wt.% P-25 TiO_2-added synthesized TiO_2	400	380, 410	3.26, 3.02
5 wt.% P-25 TiO_2-added synthesized TiO_2		380, 410	3.26, 3.02
7 wt.% P-25 TiO_2-added synthesized TiO_2		385, 415	3.22, 2.99
5 wt.% P-25 TiO_2-added synthesized TiO_2	400	380, 410	3.26, 3.02
	450	380, 410	3.26, 3.02
	500	380, 415	3.26, 2.99

4.1.4 XRD Results

The X-ray analysis was used to identify the crystalline phases of the investigated photocatalysts. The XRD patterns of the synthesized mesoporous-assembled TiO_2 photocatalyst films calcined at different temperatures are shown in Figure 4.6. It should be noted that several small diffraction peaks observed throughout the diffraction angles belong to the glass plate, as comparatively shown in Figure 4.6. The XRD patterns show crystalline structure of the pure anatase TiO_2 phase due to the presence of a diffraction peak at 2θ of about 25.2°, which represents the index of anatase (101) plane (JCPDS Card No. 21-1272) (Smith, 1960). The XRD patterns of the 5 wt.% P-25 TiO_2-addition synthesized mesoporous-assembled TiO_2 photocatalyst films calcined at different temperatures

are also shown in Figure 4.7. It can be seen that the increase in calcination temperature increased the TiO_2 peak intensity, reasonably due to the growth of TiO_2 crystallites. In addition, Figure 4.8 shows the XRD patterns of the synthesized mesoporous-assembled TiO_2 photocatalyst films calcined at 400 °C with P-25 TiO_2 addition at different contents. Although the P-25 TiO_2 possessing both the anatase and rutile TiO_2 phase (rutile content of 23%) was incorporated to synthesized mesoporous-assembled TiO_2, the crystalline structure of the mixture was still the anatase TiO_2. There was no observed diffraction peak of rutile TiO_2 phase at 2θ of about 27.4°, which represents the index of rutile (110) plane (JCPDS Card No. 21-1276) (Smith, 1960), possibly due to low P-25 TiO_2. Hence, the incorporated P-25 TiO_2 at such low contents did not significantly affect the crystalline structure of the P-25 TiO_2-added synthesized mesoporous-assembled TiO_2 photocatalysts.

The crystallite sizes of all the synthesized photocatalysts were also estimated from the line broadening of the correlative diffraction peak of the anatase (101) crystalline phase by using the Sherrer equation (Cullity, 1978) (Eq. 4.4):

$$L = \frac{k\lambda}{\beta\cos(\theta)} \tag{4.4}$$

where L is the crystallite size, k is the Sherrer constant usually taken as 0.89, λ is the wavelength of the X-ray radiation (0.15418 nm for Cu Kα), β is the full width at half maximum (FWHM) of the diffraction peak measured at 2θ, and θ is the diffraction angle. Table 4.3 summarizes the results of TiO_2 crystallite size of the synthesized mesoporous-assembled TiO_2 photocatalysts without and with P-25 TiO_2 addition calcined at different temperatures. The increase in added P-25 TiO_2 content caused the increase in TiO_2 crystallite size; however, the increase in calcination temperature in the investigated range of 400-500 °C did not significantly affect the TiO_2 crystallite size of the synthesized mesoporous-assembled TiO_2 photocatalysts without and with 5 wt.% P-25 TiO_2 addition.

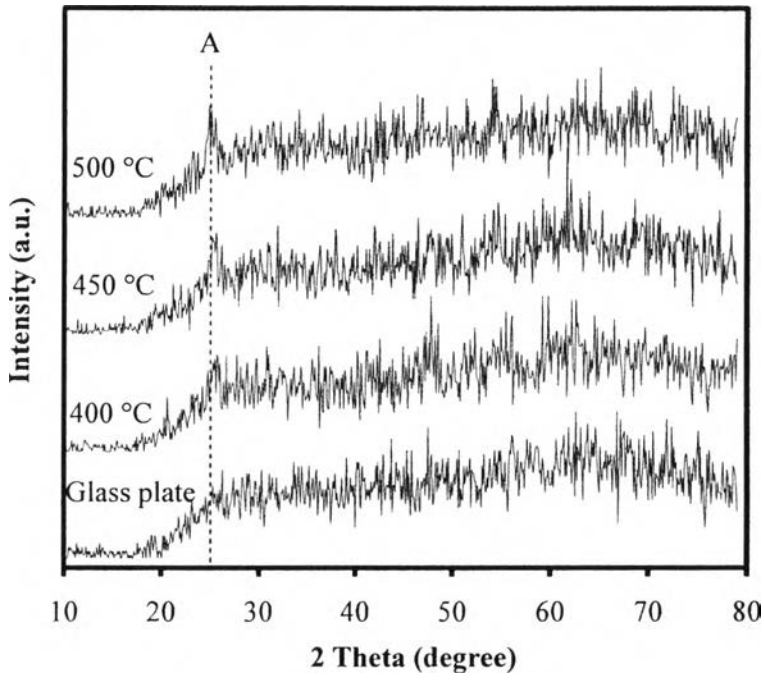

Figure 4.6 XRD patterns of the synthesized mesoporous-assembled TiO_2 photocatalyst films coated on glass plate and calcined at different temperatures.

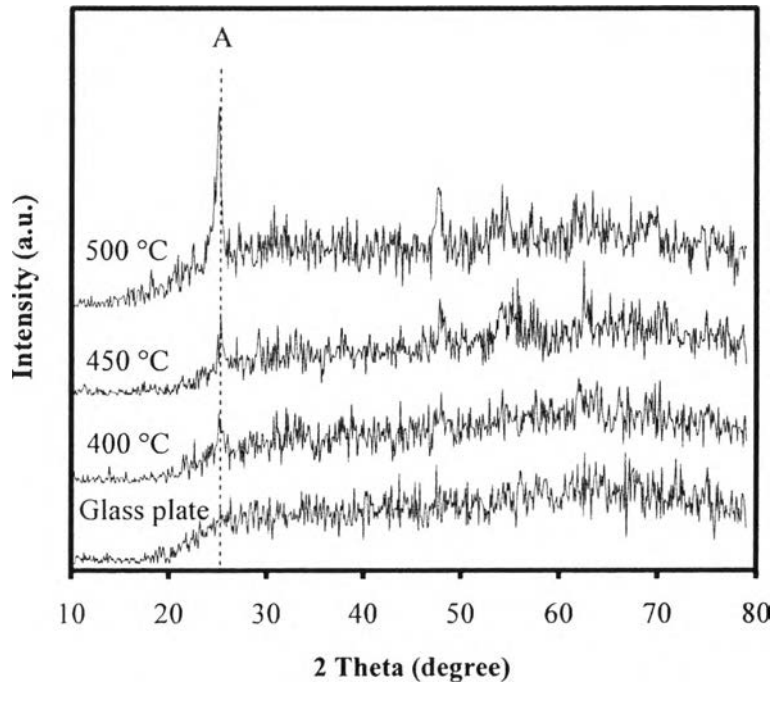

Figure 4.7 XRD patterns of the 5 wt.% P-25 TiO_2-added synthesized mesoporous-assembled TiO_2 photocatalyst films coated on glass plate and calcined at different temperatures.

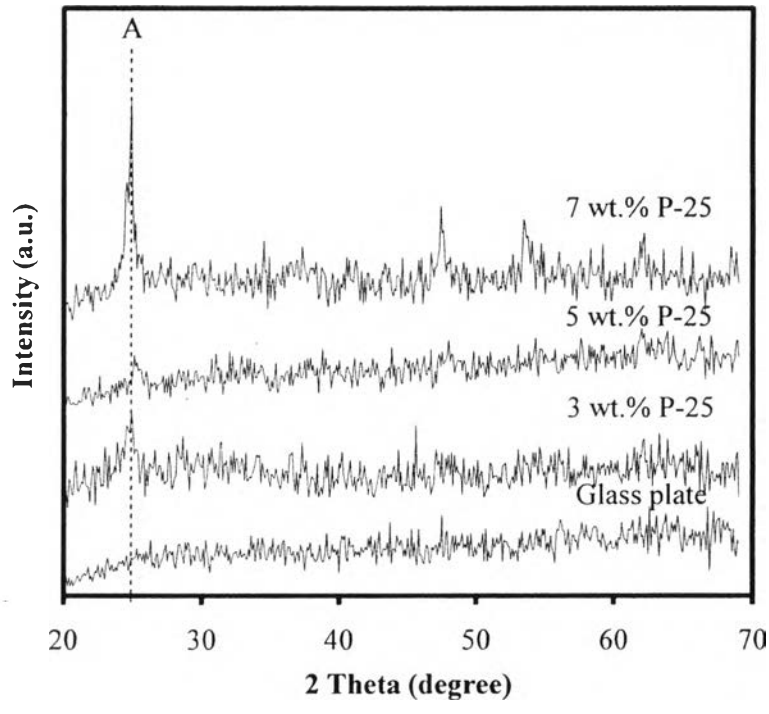

Figure 4.8 XRD patterns of the synthesized mesoporous-assembled TiO_2 photocatalyst films coated on glass plate calcined at 400 °C with P-25 TiO_2 addition at different contents.

Table 4.3 Crystallite size results of the synthesized mesoporous-assembled TiO_2 photocatalysts without and with P-25 TiO_2 addition calcined at different temperatures

Photocatalyst	Calcination temperature (°C)	Anatase (101) crystallite size (nm)
Synthesized TiO_2	400	8.59
	450	8.60
	500	8.66
3 wt.% P-25 TiO_2-added synthesized TiO_2	400	9.57
5 wt.% P-25 TiO_2-added synthesized TiO_2		14.68
7 wt.% P-25 TiO_2-added synthesized TiO_2		17.06
5 wt.% P-25 TiO_2-added synthesized TiO_2	400	14.68
	450	14.71
	500	14.73

4.1.5 SEM Results

The SEM images (top and cross-sectional views) of the synthesized mesoporous-assembled TiO_2 photocatalyst films without and with 5 wt.% P-25 TiO_2 addition are shown in Figures 4.9 and 4.10, respectively. The top-viewed SEM image of the synthesized mesoporous-assembled TiO_2 photocatalyst film without P-25 TiO_2 addition as shown in Figure 4.9 reveals that the quite uniform-size particles were observed in the form of aggregated clusters consisting of many nanoparticles. This nanoparticle aggregation can be possibly the cause of the mesoporous-assembled structure formation in the synthesized photocatalysts. In contrast, the top-viewed SEM image of the synthesized mesoporous-assembled TiO_2 photocatalyst film with 5 wt.% P-25 TiO_2 addition as shown in Figure 4.10 reveals the presence of

agglomerated clusters formed by an aggregation of the P-25 TiO_2 nanoparticles (larger particle size) with the synthesized TiO_2 nanoparticles (smaller particle size), with an insertion of the aggregated P-25 TiO_2 nanoparticles among the aggregated synthesized TiO_2 nanoparticles. Moreover, the results of film thickness of all the investigated TiO_2 films obtained from the cross-sectional viewed SEM images are summarized in Table 4.4. It can be seen that at any given calcination temperature, the added 5 wt.% P-25 TiO_2 favorably helped increase the thickness of the synthesized mesoporous-assembled TiO_2 film as compared to the film without P-25 TiO_2 addition for 1-layer coating. In addition, the increases in number of coated TiO_2 layers and added P-25 TiO_2 content caused an increase in the thickness of the TiO_2 films possibly due to the increased adhesion capability of the films and the increased amount of coated TiO_2.

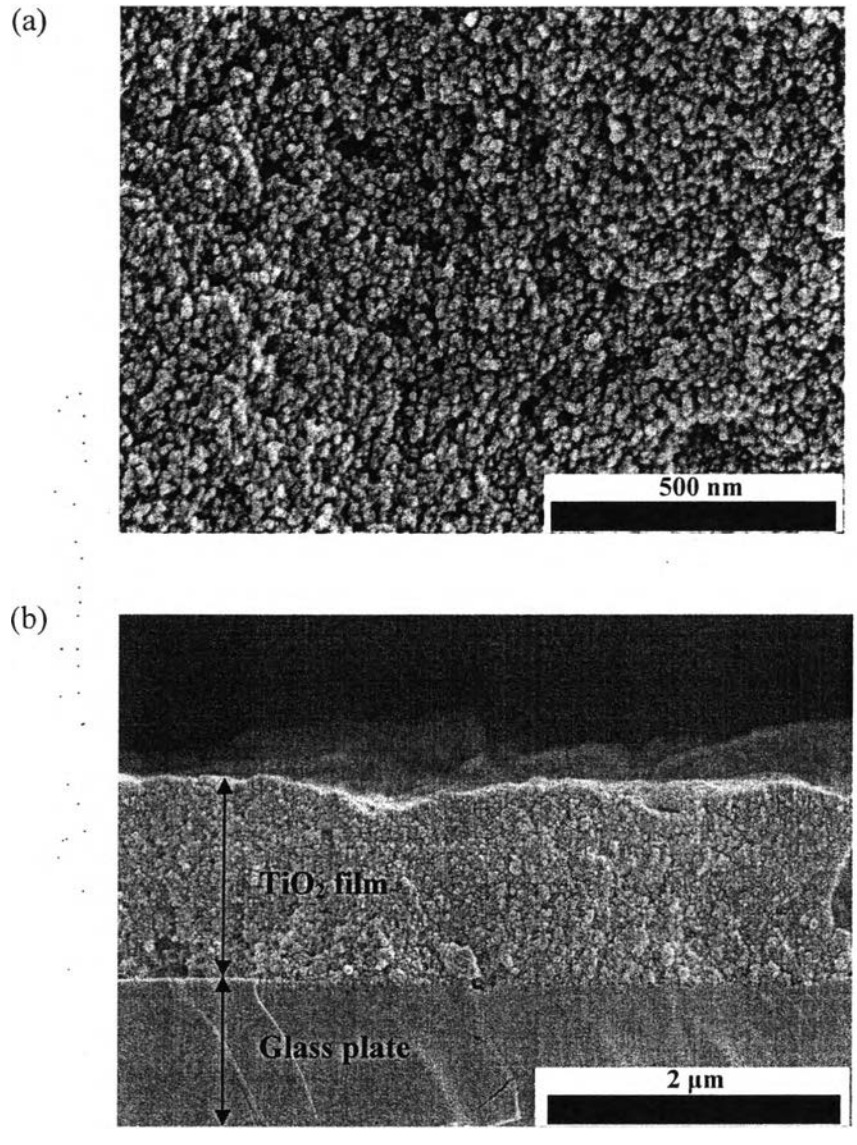

Figure 4.9 SEM images of the synthesized mesoporous-assembled TiO_2 photocatalyst film calcined at 400 °C with 1-layer coating: (a) top view and (b) cross-sectional view.

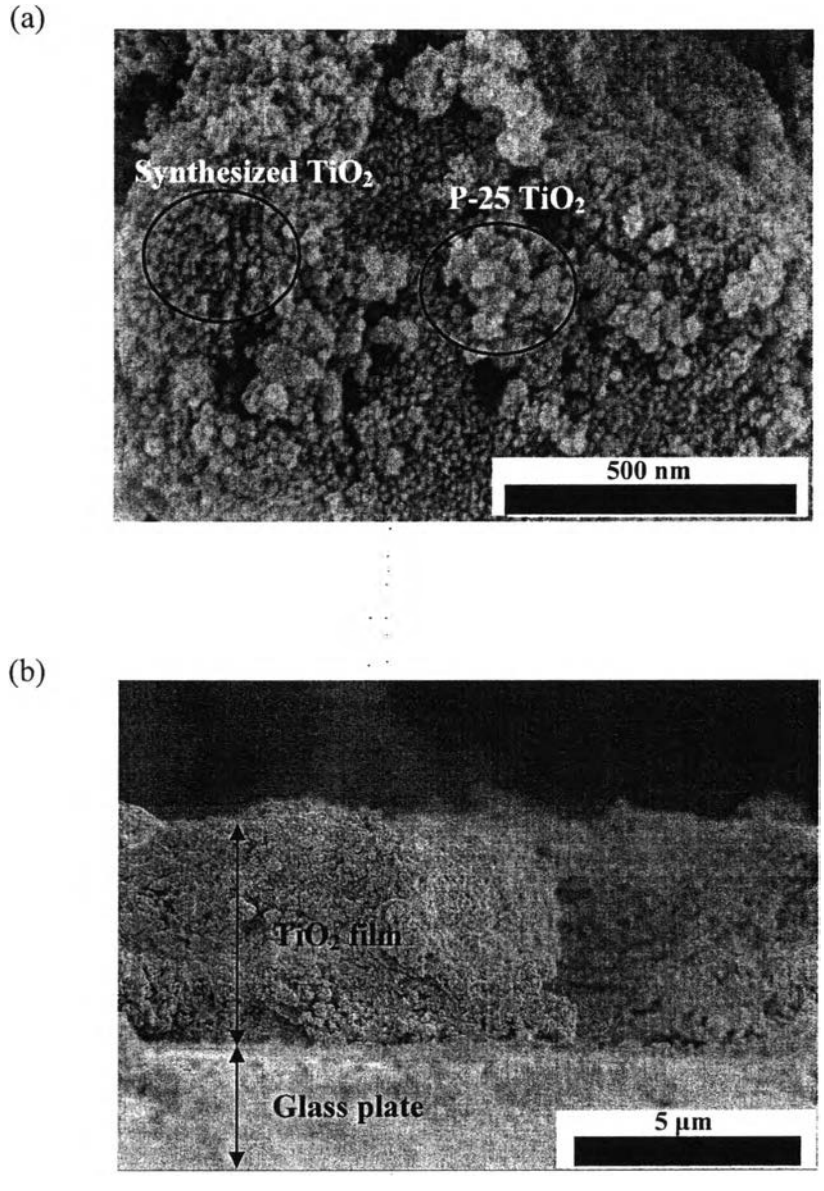

Figure 4.10 SEM images of the 5 wt.% P-25 TiO_2-added synthesized mesoporous-assembled TiO_2 photocatalyst film calcined at 400 °C with 1-layer coating: (a) top view and (b) cross-sectional view.

Table 4.4 TiO_2 film thickness results of the synthesized mesoporous-assembled TiO_2 photocatalyst films without and with P-25 TiO_2 addition calcined at different temperatures

Photocatalyst	Calcination temperature (°C)	Number of coated TiO_2 layers	Thickness of TiO_2 film (μm)
Synthesized TiO_2	400	1	1.37
	450		2.24
	500		1.98
Synthesized TiO_2	400	1	1.37
		2	11.8
		3	22.5
3 wt.% P-25 TiO_2-added synthesized TiO_2	400	1	1.24
5 wt.% P-25 TiO_2-added synthesized TiO_2			4.96
7 wt.% P-25 TiO_2-added synthesized TiO_2			5.83
5 wt.% P-25 TiO_2-added synthesized TiO_2	400	1	4.96
	450		4.75
	500		4.51
5 wt.% P-25 TiO_2-added synthesized TiO_2	400	1	4.96
		2	21.4
		3	33.7
		4	46.4

4.1.6 TEM Results

The morphologies and particle sizes of the synthesized mesoporous-assembled TiO_2 photocatalyst without and with P-25 TiO_2 addition were investigated by the TEM analysis, as exemplified in Figure 4.11. It can be comparatively seen that when the P-25 TiO_2 was added to the synthesized mesoporous-assembled TiO_2, the existence of the P-25 TiO_2 nanoparticles (larger particle size) with the synthesized mesoporous-assembled TiO_2 nanoparticles (smaller particle size) was clearly observed, with their aggregations as previously seen by the SEM analysis. The average particle sizes of the mesoporous-assembled TiO_2 and the P-25 TiO_2 photocatalysts were in the range of 5-10 and 15-25 nm, respectively, where the observed particle sizes are in good accordance with the crystallite sizes estimated from the XRD analysis (Table 4.3).

(a)

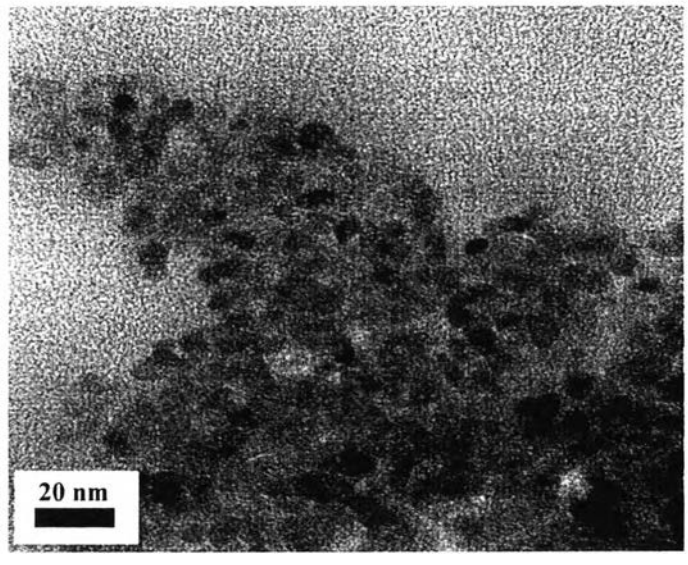

(b)

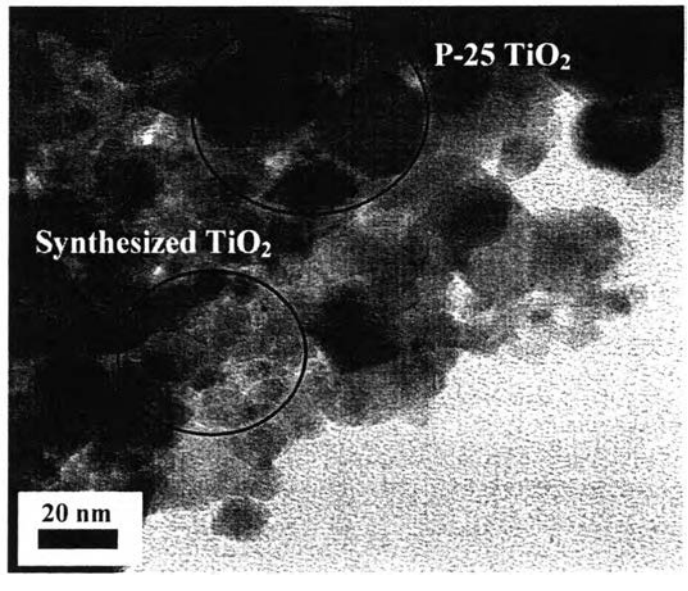

Figure 4.11 TEM images of the synthesized mesoporous-assembled TiO_2 photocatalysts scraped from the TiO_2 film-coated glass plates: (a) without and (b) with 5 wt.% P-25 TiO_2 addition (400 °C calcination temperature).

4.1.7 Amount of TiO_2 Photocatalyst Coated on Glass Plate

The amounts of the synthesized mesoporous-assembled TiO_2 photocatalysts without and with P-25 TiO_2 addition scraped from the TiO_2 film-coated glass plates are shown in Table 4.5. It can be comparatively seen that at any given calcination temperature, when the P-25 TiO_2 photocatalyst was added to the synthesized mesoporous-assembled TiO_2 photocatalyst, the amount of coated TiO_2 powders was higher than that without P-25 TiO_2 addition. This clearly confirms an important role of the P-25 TiO_2 photocatalyst in helping increase the film thickness of the synthesized mesoporous-assembled TiO_2 photocatalyst. Moreover, the increase in number of coated TiO_2 layers significantly enhanced the amount of coated TiO_2 powders for the synthesized mesoporous-assembled TiO_2 photocatalysts both without and with 5 wt.% P-25 TiO_2 addition, as expected. In contrast, the increase in calcination temperature in the investigated range of 400-500 °C only slightly affected the amount of coated TiO_2 powders.

Table 4.5 Amount of the synthesized mesoporous-assembled TiO_2 photocatalysts without and with P-25 TiO_2 addition coated on glass plate and calcined at different temperatures

Photocatalyst	Calcination temperature (°C)	Number of coated TiO_2 layers	Weight of TiO_2 powders on 8 glass plates (mg)
Synthesized TiO_2	400	1	26.8
	450		31.8
	500		42.2
Synthesized TiO_2	400	1	26.8
		2	61.2
		3	110.8
3 wt.% P-25 TiO_2-added synthesized TiO_2	400	1	91.8
5 wt.% P-25 TiO_2-added synthesized TiO_2			110.2
7 wt.% P-25 TiO_2-added synthesized TiO_2			162.5
5 wt.% P-25 TiO_2-added synthesized TiO_2	400	1	110.2
	450		89.2
	500		103.4
5 wt.% P-25 TiO_2-added synthesized TiO_2	400	1	110.2
		2	254.8
		3	496.0
		4	796.2

4.1.8 AFM Results

AFM was used to investigate the surface topology and roughness of the glass plate without and with NaOH treatment prior to being coated with the TiO_2 photocatalysts, as well as those of the synthesized mesoporous-assembled TiO_2 photocatalyst films coated on glass plate without and with 5 wt.% P-25 TiO_2 addition. Figure 4.12 shows the 3-dimensional AFM images of the glass plates without and with NaOH treatment. It can be clearly seen that the glass plate with NaOH treatment exhibited rougher surface texture with higher porosity than that without NaOH treatment. The change in the surface roughness was determined from the AFM images, as shown Table 4.6. The roughness of the glass plate was verified to significantly increase after the glass plate was treated with the NaOH aqueous solution. Hence, this increased surface roughness of the glass plate led to an enhanced adhesion capability of the TiO_2 films, as clearly shown above for the results of SEM analysis and amount of coated TiO_2; whereas, the easy peel-off of the TiO_2 films was experimentally observed from the surface of NaOH-untreated glass plate placed in the continuously agitated AB dye solution during the photocatalytic activity tests. Figure 4.12 also shows the 3-dimensional AFM images of the synthesized mesoporous-assembled TiO_2 photocatalyst films coated on glass plate without and with P-25 TiO_2 addition, where their surface roughness is summarized in Table 4.7. The surface of all the samples consisted of aggregated clusters consisting of many nanoparticles, as shown above from the SEM results (Figures 4.9 and 4.10). It can be observed that the addition of P-25 TiO_2 to the synthesized mesoporous-assembled TiO_2 resulted in an increase in the surface roughness with high mountains and deep valleys induced by an aggregation of the P-25 TiO_2 nanoparticles with the synthesized mesoporous-assembled TiO_2 ones, while an increase in the surface roughness with increasing calcination temperature could be possibly due to a more surface topology shrinkage upon a more severe thermal treatment.

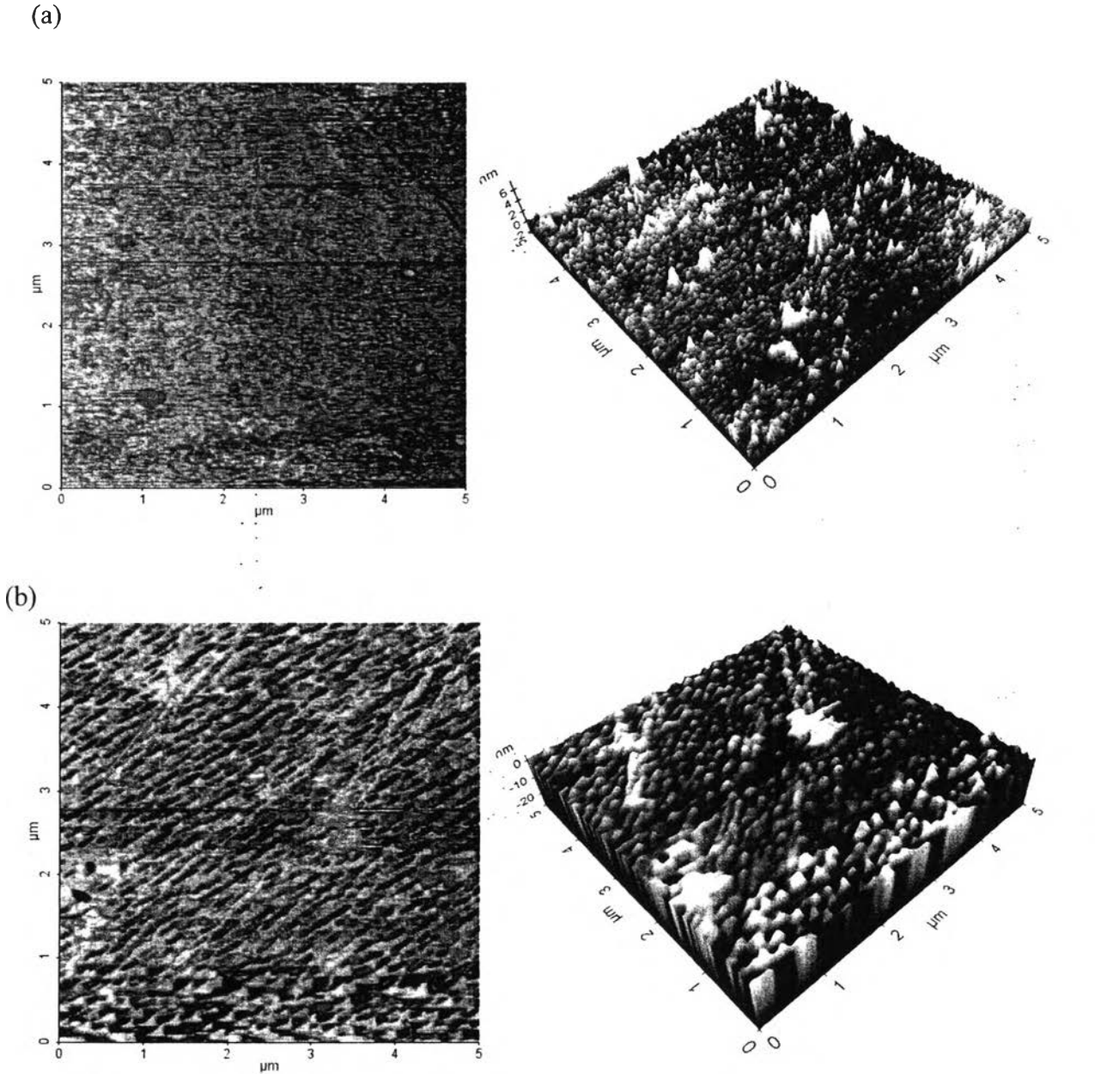

Figure 4.12 3-Dimensional AFM images (5×5 µm surface plots) of the glass plates: (a) without and (b) with NaOH treatment, and of the synthesized mesoporous-assembled TiO_2 films coated on glass plate calcined at 400 °C: (c) without and (d) with 5 wt.% P-25 TiO_2 addition.

(c)

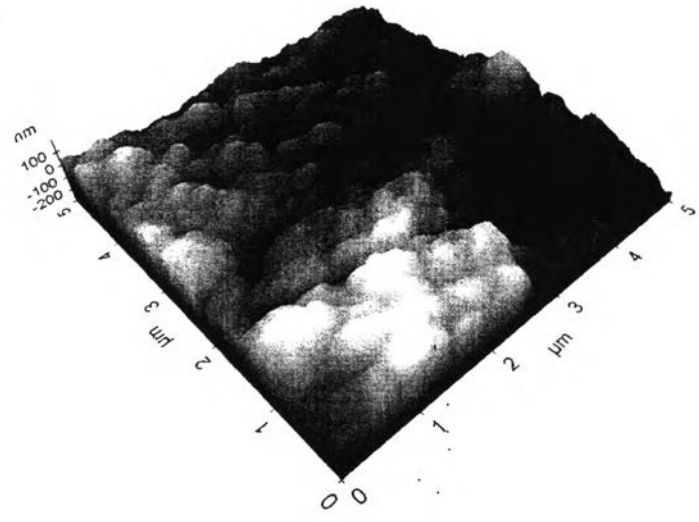

(d)

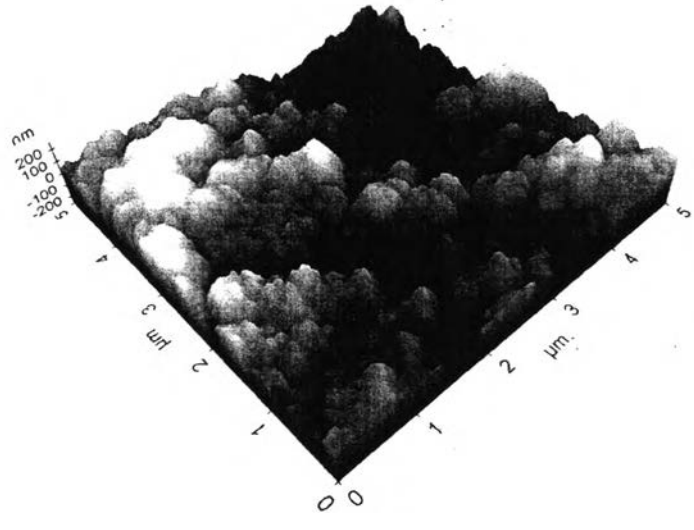

Figure 4.12 (Continued) 3-Dimensional AFM images (5×5 μm surface plots) of the glass plates: (a) without and (b) with NaOH treatment, and of the synthesized mesoporous-assembled TiO_2 films coated on glass plate calcined at 400 °C: (c) without and (d) with 5 wt.% P-25 TiO_2 addition.

Table 4.6 Surface roughness results of glass plate without and with NaOH treatment

Glass plate	Surface roughness (nm)
Without NaOH treatment	0.303
With NaOH treatment	0.987

Table 4.7 Surface roughness results of the synthesized mesoporous-assembled TiO_2 photocatalyst films coated on glass plate without and with 5 wt.% P-25 TiO_2 addition

Photocatalyst	Calcination temperature (°C)	Surface roughness (nm)
Synthesized TiO_2	400	58.0
5 wt.% P-25 TiO_2-added synthesized TiO_2	400	67.4
	450	98.7
	500	156.1

4.2 Photocatalytic AB Dye Degradation Results

4.2.1 UV-Visible Spectroscopy

UV-visible spectroscopy was used to investigate the effects of various operating parameters on the AB dye degradation performance of all the synthesized mesoporous-assembled TiO_2 photocatalyst films without and with P-25 TiO_2 addition. The UV-visible spectrum of AB dye solution reveals the λ_{max} value at 619 nm, as shown in Figure 4.13, and the decrease in its λ_{max} value was used to evaluate the degradation performance, as exemplified in Figure 4.14.

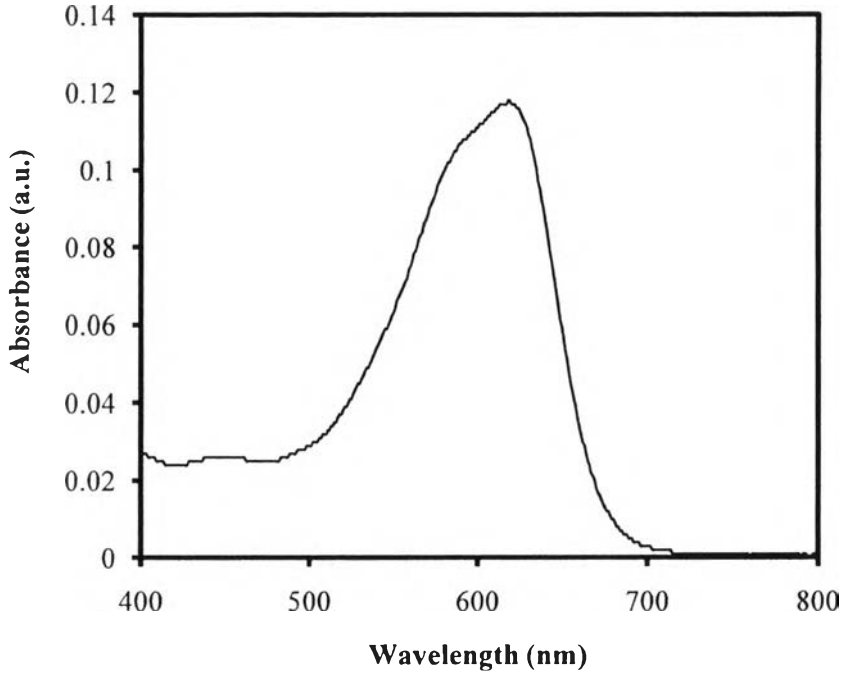

Figure 4.13 UV-visible spectrum of AB dye solution.

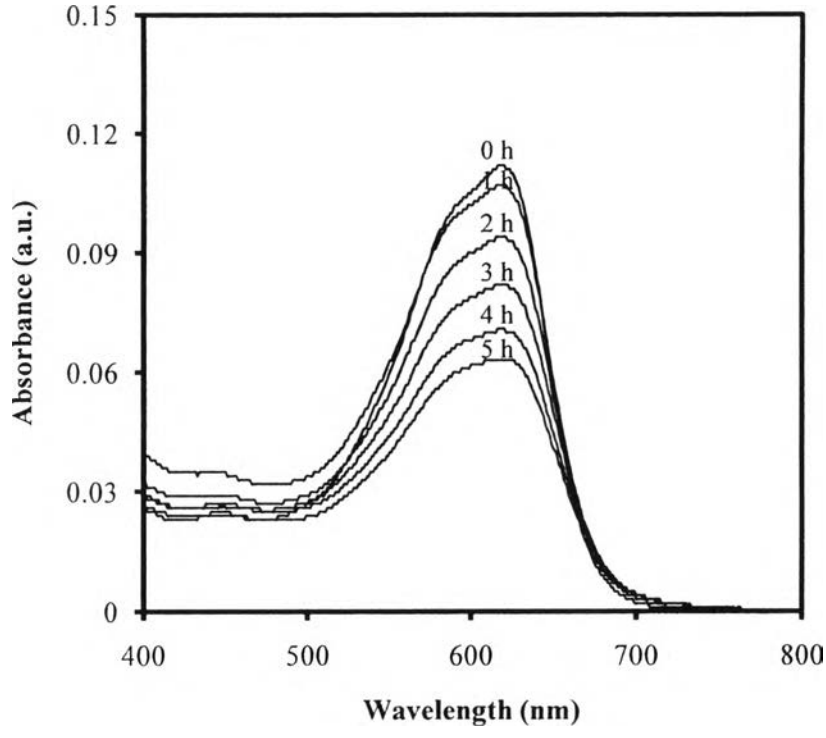

Figure 4.14 UV-visible spectra of AB dye solution as a function of irradiation time during the course of photocatalytic degradation using the synthesized mesoporous-assembled TiO_2 photocatalyst film (total reaction mixture volume, 500 ml; initial AB concentration, 10 mg/l; initial solution pH, 5.04; number of coated TiO_2 layer, 1 layer; and number of TiO_2-coated glass plate, 8 plates.)

4.2.2 Effect of Calcination Temperature of the Synthesized Mesoporous-Assembled TiO_2 Photocatalyst Film

The effect of calcination temperature of the synthesized mesoporous-assembled TiO_2 photocatalyst film on the photocatalytic AB dye degradation was first investigated. The results of photocatalytic AB dye degradation over the synthesized mesoporous-assembled TiO_2 photocatalyst film calcined in the temperature range of 400 to 500 °C at the controlled number of coated TiO_2 layer of 1 layer are shown in Figures 4.15 and 4.16. It could be seen that the AB dye degradation efficiency and the reaction rate constant only slightly increased with increasing calcination temperature and reached maximum values at 500 °C, and they seemed not to significantly change. Even though the specific surface area of the synthesized mesoporous-assembled TiO_2 photocatalyst decreased with increasing

calcination temperature (Table 4.1), the TiO_2 film thickness and the amount of coated TiO_2 tended to conversely increase (Tables 4.4 and 4.5). This may, in overall, result in similar number of surface active sites for photocatalytic reaction at different calcination temperatures. Hence, the observed slight increase in the photocatalytic activity at a higher calcination temperature could be possibly explained by band gap energy results (Table 4.2), showing the lowest value for the synthesized mesoporous-assembled TiO_2 photocatalyst film calcined at 500 °C. This indicated that this photocatalyst required a lower light energy for band gap excitation and consequently generated a higher number of charge carriers, leading to its higher photocatalytic activity than the others.

Due to the limitation of active sites available, the increase in number of coated TiO_2 layers (i.e. the increase in film thickness) was expected to enhance the photocatalytic activity and was further investigated at various calcination temperatures. It was experimentally observed that the second layer of the mesoporous-assembled TiO_2 film after the calcination at temperatures of 450 and 500 °C easily peeled off from the glass plate during the photocatalytic activity tests; therefore, both calcination temperatures could not be used to study the effect of increasing coated TiO_2 layers. For this reason, the calcination temperature of 400 °C could only be used in further experiments.

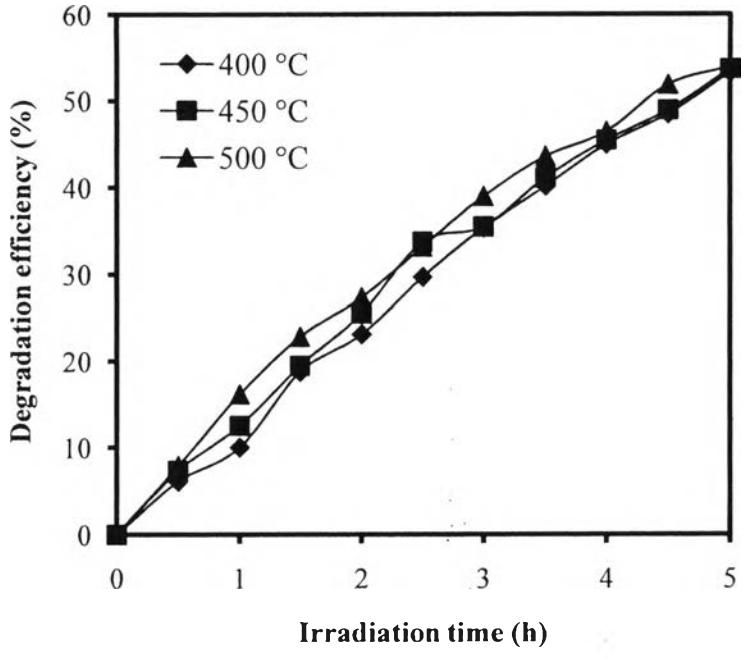

Figure 4.15 Effect of calcination temperature of the synthesized mesoporous-assembled TiO_2 photocatalyst film on AB dye degradation efficiency (total reaction mixture volume, 500 ml; initial AB dye concentration, 10 mg/l; initial solution pH, 5.04; number of coated TiO_2 layer, 1 layer; number of TiO_2-coated glass plate, 8 plates; and irradiation time, 5 h).

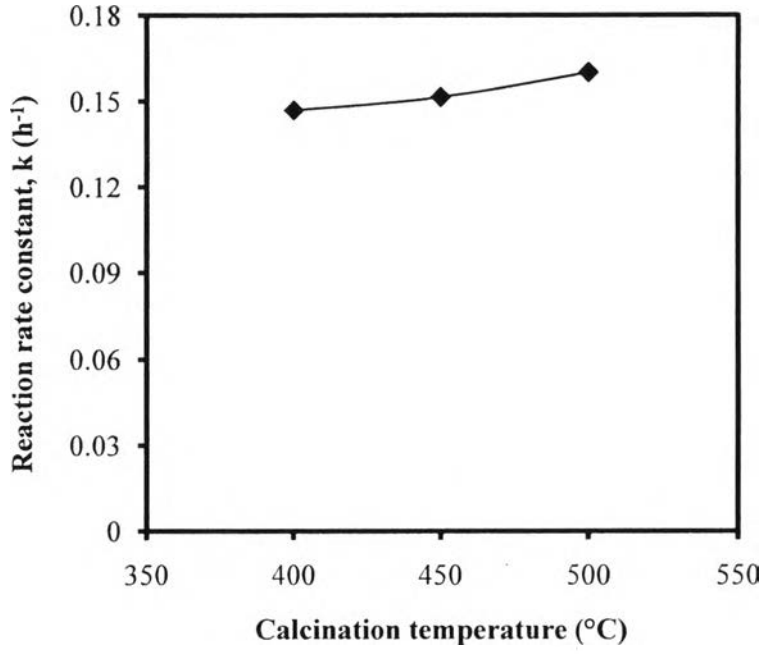

Figure 4.16 Effect of calcination temperature of the synthesized mesoporous-assembled TiO_2 photocatalyst film on reaction rate constant for AB dye degradation (total reaction mixture volume, 500 ml; initial AB dye concentration, 10 mg/l; initial solution pH, 5.04; number of coated TiO_2 layer, 1 layer; number of TiO_2-coated glass plate, 8 plates; and irradiation time, 5 h).

4.2.3 Effect of Number of Coated TiO_2 Layers of the Synthesized Mesoporous-Assembled TiO_2 Photocatalyst Film

The effect of number of coated TiO_2 layers of the synthesized mesoporous-assembled TiO_2 photocatalyst film calcined at 400 °C on the photocatalytic AB dye degradation was next investigated. The results of photocatalytic degradation over the synthesized mesoporous-assembled TiO_2 photocatalyst film with different coated TiO_2 layers are shown in Figures 4.17 and 4.18. It was clearly seen that with increasing number of coated TiO_2 layers, the AB dye degradation efficiency and the reaction rate constant increased more substantially as compared to the case of increasing calcination temperature, and they reached maximum values at three coated TiO_2 layers. According to the TiO_2 film thickness results (Table 4.4), the increase in the number of coated TiO_2 layers caused an increase in the TiO_2 film thickness, and this accordingly resulted in the increased

amount of coated TiO_2 (Table 4.5) and thus the increased available surface active sites and light scattering probability to generate more charge carriers for photocatalytic reaction, leading to the observed higher photocatalyst activity. However, the number of coated TiO_2 layers higher than 3 layers could not be achieved due to the easy peel-off of the TiO_2 film from the glass plate during the photocatalytic reaction. This might result from the too thick multilayer TiO_2 films, and the adhesion capability between layers was extremely weak.

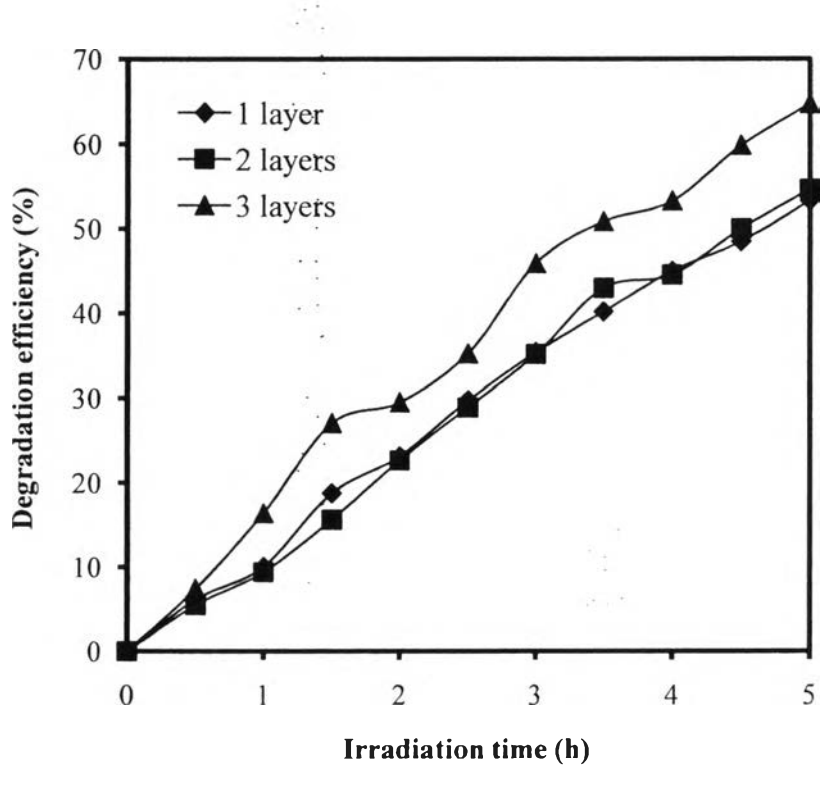

Figure 4.17 Effect of number of coated TiO_2 layers of the synthesized mesoporous-assembled TiO_2 photocatalyst film on AB dye degradation efficiency (total reaction mixture volume, 500 ml; initial AB dye concentration, 10 mg/l; initial solution pH, 5.04; calcination temperature, 400 °C; number of TiO_2-coated glass plate, 8 plates; and irradiation time, 5 h).

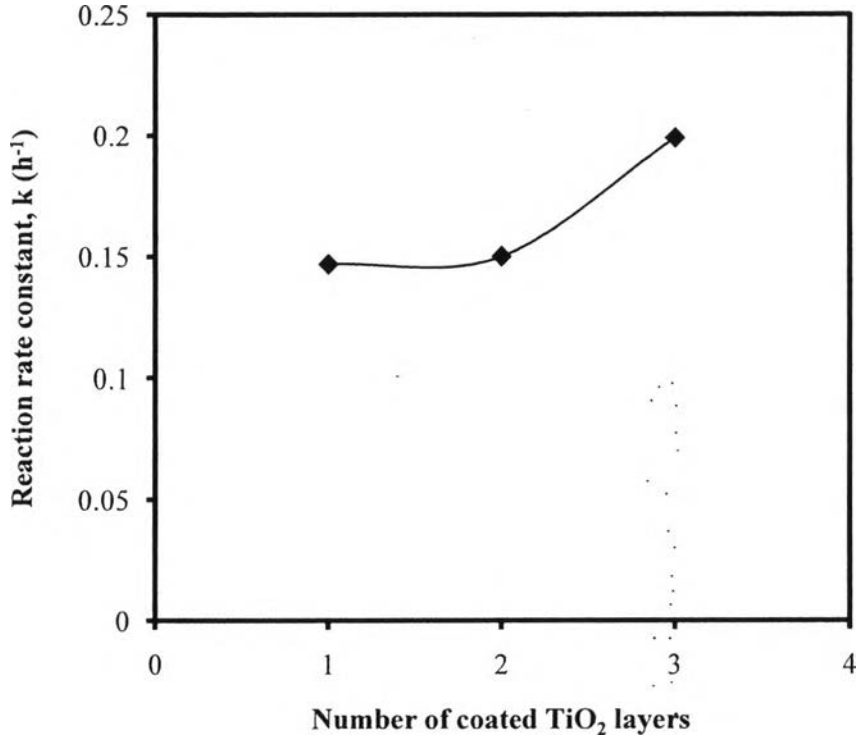

Figure 4.18 Effect of number of coated TiO_2 layers of the synthesized mesoporous-assembled TiO_2 photocatalyst film on reaction rate constant for AB dye degradation (total reaction mixture volume, 500 ml; initial AB dye concentration, 10 mg/l; initial solution pH, 5.04; calcination temperature, 400 °C; number of TiO_2-coated glass plate, 8 plates; and irradiation time, 5 h).

4.2.4 Effect of P-25 TiO_2 Content Added to the Synthesized Mesoporous-Assembled TiO_2 Photocatalyst

The effect of P-25 TiO_2 content added to the synthesized mesoporous-assembled TiO_2 photocatalyst film on the photocatalytic AB dye degradation was further investigated, aiming at increasing the adhesion capability in order to obtain thicker TiO_2 films. The results of photocatalytic degradation over the P-25 TiO_2-added synthesized mesoporous-assembled TiO_2 photocatalyst film with 1-layer coating calcined at 400 °C are shown in Figures 4.19 and 4.20. It was found that the AB dye degradation efficiency and the reaction rate constant increased with increasing added P-25 content to reach maximum values at 5 wt.%, but they

decreased with further increasing added P-25 TiO_2 content up to 7 wt.%. From the N_2 adsorption-desorption results (Table 4.1), the addition of P-25 TiO_2 with an appropriate amount of 5 wt.% led to a maximum specific surface area and total pore volume of the P-25 TiO_2-added synthesized mesoporous-assembled TiO_2 photocatalyst. This indicates that the 5 wt.% P-25 TiO_2-added synthesized mesoporous-assembled TiO_2 photocatalyst possessed the highest surface active sites than the other P-25 TiO_2-added ones, resulting in its maximum photocatalytic activity. In contrast, it was found that the increase in added P-25 TiO_2 content up to 7 wt.% caused the decreases in both specific surface area and total pore volume, leading to the decrease in photocatalytic activity. In addition, even though the highest film thickness and the highest amount of coated TiO_2 were observed for the 7 wt.% P-25 TiO_2-added synthesized mesoporous-assembled TiO_2 photocatalyst film (Tables 4.4 and 4.5), this photocatalyst had comparatively high crystallite size (Table 4.3). This might increase the probability of charge carrier recombination at the bulk traps, which negatively affected the photocatalytic activity, as observed. Therefore, the added P-25 content of 5 wt.% was considered to be an optimum value to enhance the photocatalytic activity of the synthesized mesoporous-assembled TiO_2 photocatalyst film.

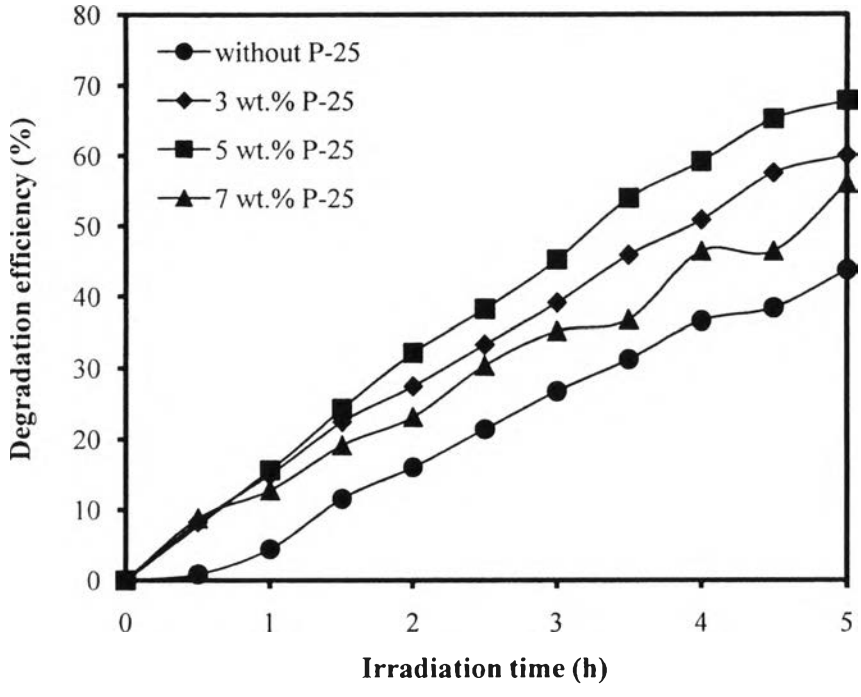

Figure 4.19 Effect of P-25 TiO_2 content added to the synthesized mesoporous-assembled TiO_2 photocatalyst film on AB dye degradation efficiency (total reaction mixture volume, 500 ml; initial AB dye concentration, 10 mg/l; initial solution pH, 5.04; calcination temperature, 400 °C; number of coated TiO_2 layer, 1 layer; number of TiO_2-coated glass plate, 8 plates; and irradiation time, 5 h).

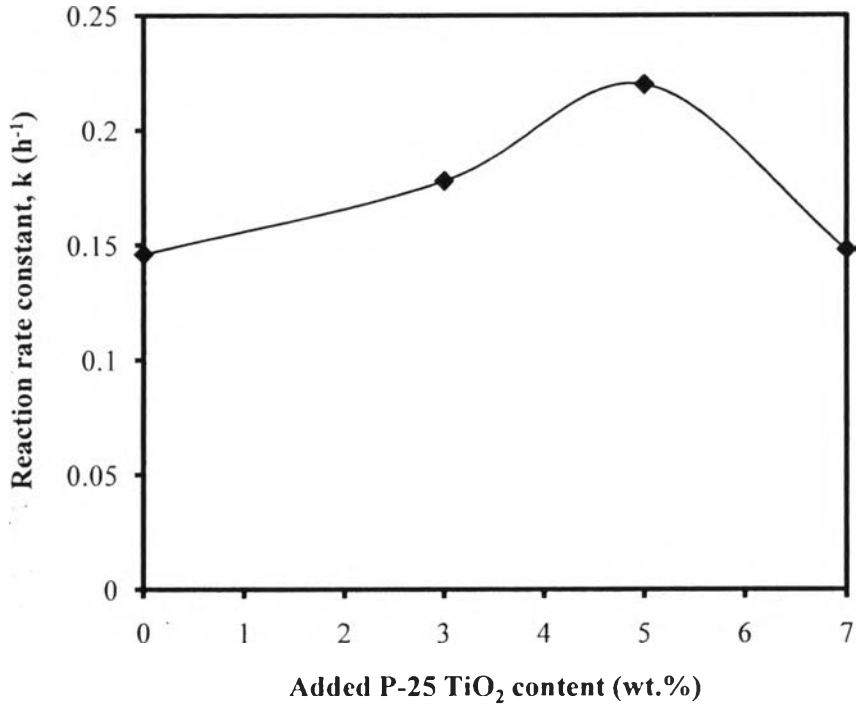

Figure 4.20 Effect of P-25 TiO_2 content added to the synthesized mesoporous-assembled TiO_2 photocatalyst film on reaction rate constant for AB dye degradation (total reaction mixture volume, 500 ml; initial AB dye concentration, 10 mg/l; initial solution pH, 5.04; calcination temperature, 400 °C; number of coated TiO_2 layer, 1 layer; number of TiO_2-coated glass plate, 8 plates; and irradiation time, 5 h).

4.2.5 Effect of Calcination Temperature of the Synthesized Mesoporous-Assembled TiO_2 Photocatalyst Film with 5 wt.% P-25 TiO_2 Addition

The effect of calcination temperature of the synthesized mesoporous-assembled TiO_2 photocatalyst film with 5 wt.% P-25 TiO_2 addition on the photocatalytic AB dye degradation was further investigated. The results of reaction rate constant for AB dye degradation over the 5 wt.% P-25 TiO_2-added synthesized mesoporous-assembled TiO_2 photocatalyst film with 1-layer coating as a function of calcination temperature are shown in Figure 4.21, as compared to the synthesized mesoporous-assembled TiO_2 film without P-25 TiO_2 addition. In the case of P-25 TiO_2 addition, the reaction rate constant gradually decreased with increasing calcination temperature; however, the opposite trend was observed in the case

without P-25 TiO_2 addition, of which the reaction rate constant slightly increased with increasing calcination temperature. Interestingly, it could be observed that at any given calcination temperature, the reaction rate constant of the synthesized mesoporous-assembled TiO_2 film with P-25 TiO_2 addition was higher than that without P-25 TiO_2 addition. The results suggest that even though the decrease in specific surface area was observed when the P-25 TiO_2 was added to the synthesized mesoporous-assembled TiO_2 film (Table 4.1), the added P-25 TiO_2 increased the efficiency of the synthesized mesoporous-assembled TiO_2 film plausibly due to the increased adhesion capability of the TiO_2 film to achieve the higher film thickness (Table 4.4) and the higher amount of coated TiO_2 (Table 4.5).

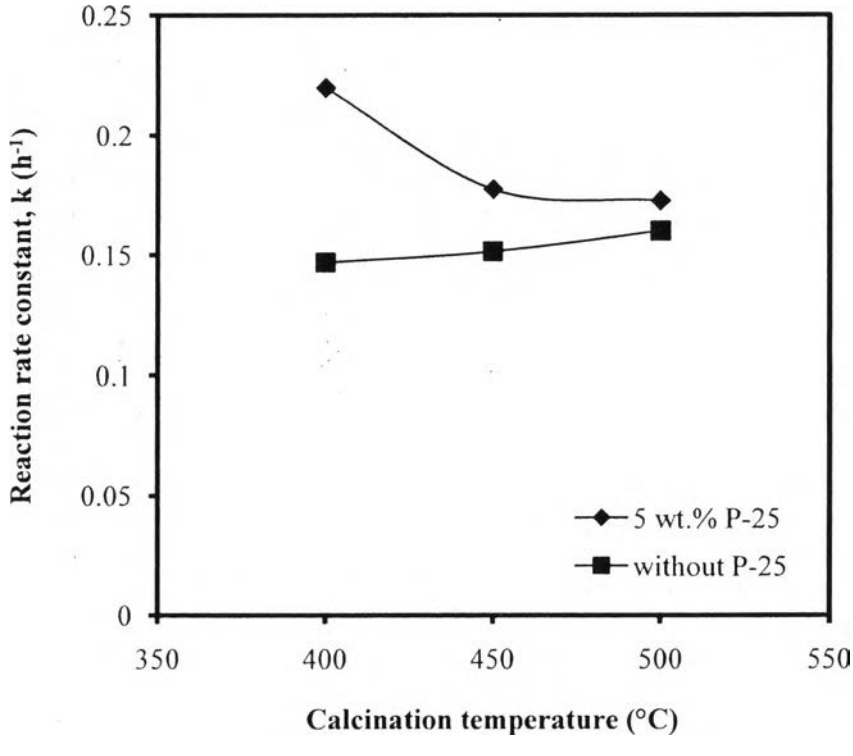

Figure 4.21 Effect of calcination temperature of the 5 wt.% P-25 TiO_2-added synthesized mesoporous-assembled TiO_2 photocatalyst film on reaction rate constant for AB dye degradation as compared to the synthesized TiO_2 photocatalyst film without P-25 TiO_2 addition (total reaction mixture volume, 500 ml; initial AB dye concentration, 10 mg/l; initial solution pH, 5.04; number of coated TiO_2 layer, 1 layer; number of TiO_2-coated glass plate, 8 plates; and irradiation time, 5 h).

4.2.6 Effect of Number of Coated TiO_2 Layers of the Synthesized Mesoporous-Assembled TiO_2 Photocatalyst Film with 5 wt.% P-25 TiO_2 Addition

The effect of number of coated TiO_2 layers of the 5 wt.% P-25 TiO_2-added synthesized mesoporous-assembled TiO_2 photocatalyst film calcined at 400 °C on the photocatalytic AB dye degradation was next investigated. The results of photocatalytic AB dye degradation over the 5 wt.% P-25 TiO_2-added synthesized mesoporous-assembled TiO_2 photocatalyst film with various coated layers are shown in Figures 4.22 and 4.23. It could be clearly observed that when the number of coated TiO_2 layers increased, the AB dye degradation efficiency and the reaction rate constant increased to reach maximum values at four coated TiO_2 layers. This is possibly because of the increased TiO_2 film thickness (Table 4.4) and the increased amount of coated TiO_2 (Table 4.5) at a higher number coated TiO_2 layers, consequently leading to the increase in surface active sites for photocatalytic reaction. Although the 5 wt.% P-25 TiO_2 was added to increase the TiO_2 film thickness, the TiO_2 film peel-off was also clearly observed at the number of coated TiO_2 layers higher than 4 layers. Therefore, an effective way to solve this peel-off limitation should be further investigated in the future work.

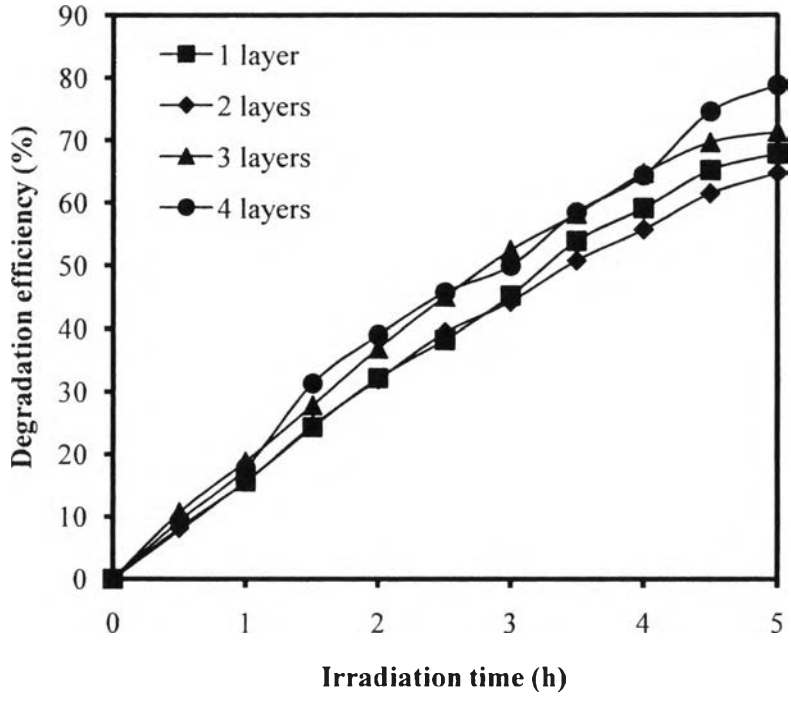

Figure 4.22 Effect of number of coated TiO_2 layers of the 5 wt.% P-25 TiO_2-added synthesized mesoporous-assembled TiO_2 photocatalyst film on AB dye degradation efficiency (total reaction mixture volume, 500 ml; initial AB dye concentration, 10 mg/l; initial solution pH, 5.04; calcination temperature, 400 °C; number of TiO_2-coated glass plate, 8 plates; and irradiation time, 5 h).

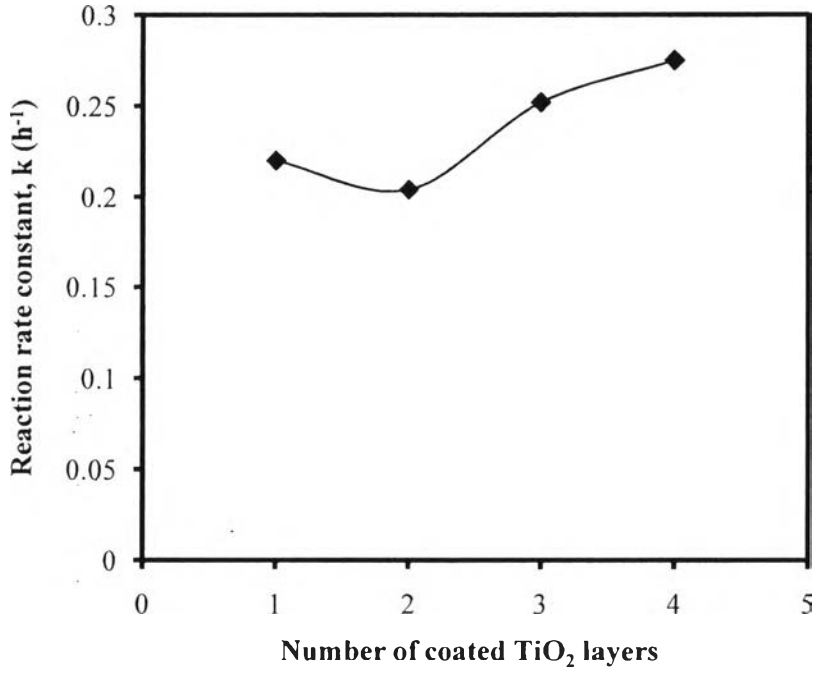

Figure 4.23 Effect of number of coated TiO_2 layers of the 5 wt.% P-25 TiO_2-added synthesized mesoporous-assembled TiO_2 photocatalyst film on reaction rate constant for AB dye degradation (total reaction mixture volume, 500 ml; initial AB dye concentration, 10 mg/l; initial solution pH, 5.04; calcination temperature, 400 °C; number of TiO_2-coated glass plate, 8 plates; and irradiation time, 5 h).

4.2.7 Effect of Recyclability of the Synthesized Mesoporous-Assembled TiO_2 Photocatalyst Film with 5 wt.% P-25 TiO_2 Addition

The effect of recyclability of the synthesized mesoporous-assembled TiO_2 photocatalyst film with 5 wt.% P-25 TiO_2 addition on the photocatalytic AB dye degradation was investigated for three consecutive cycles, without a chemical or thermal post-treatment of the film after each cycle. The results of photocatalytic AB dye degradation over the 5 wt.% P-25 TiO_2-added synthesized mesoporous-assembled TiO_2 photocatalyst film with 4-layer coating are shown in Figures 4.24 and 4.25. It could be clearly observed that the synthesized mesoporous-assembled TiO_2 photocatalyst film with 5 wt.% P-25 TiO_2 addition exhibited the almost unchanged photocatalytic AB dye degradation performance for

three consecutive cycles. This indicates the acceptably high stability of the film for the photocatalytic dye degradation application.

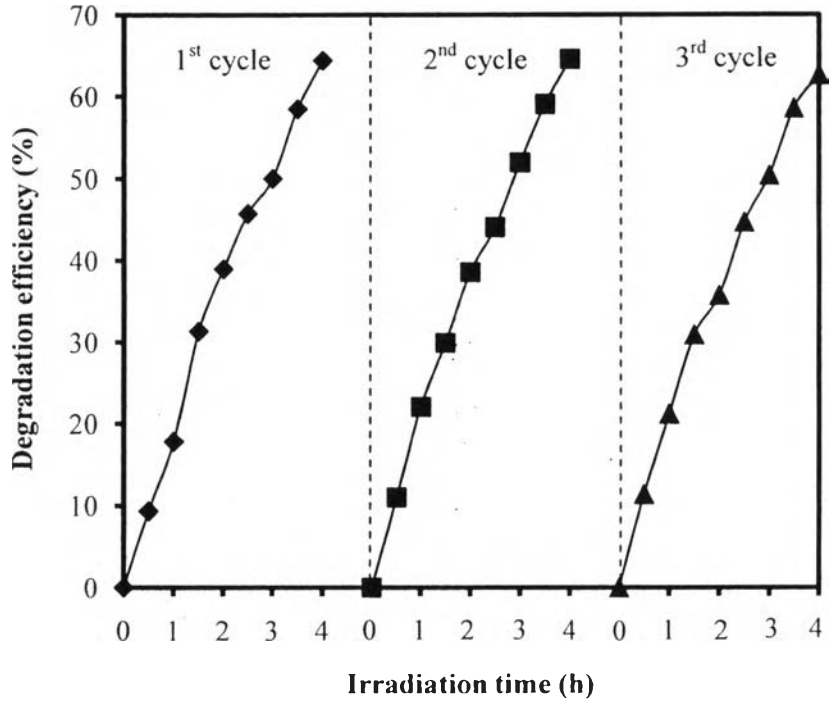

Figure 4.24 Effect of recyclability of the synthesized mesoporous-assembled TiO_2 photocatalyst film with 5 wt.% P-25 TiO_2 addition on AB dye degradation efficiency (total reaction mixture volume, 500 ml; initial AB dye concentration, 10 mg/l; initial solution pH, 5.04; calcination temperature, 400 °C; number of coated TiO_2 layer, 4 layer; number of TiO_2-coated glass plate, 8 plates; and irradiation time, 4 h).

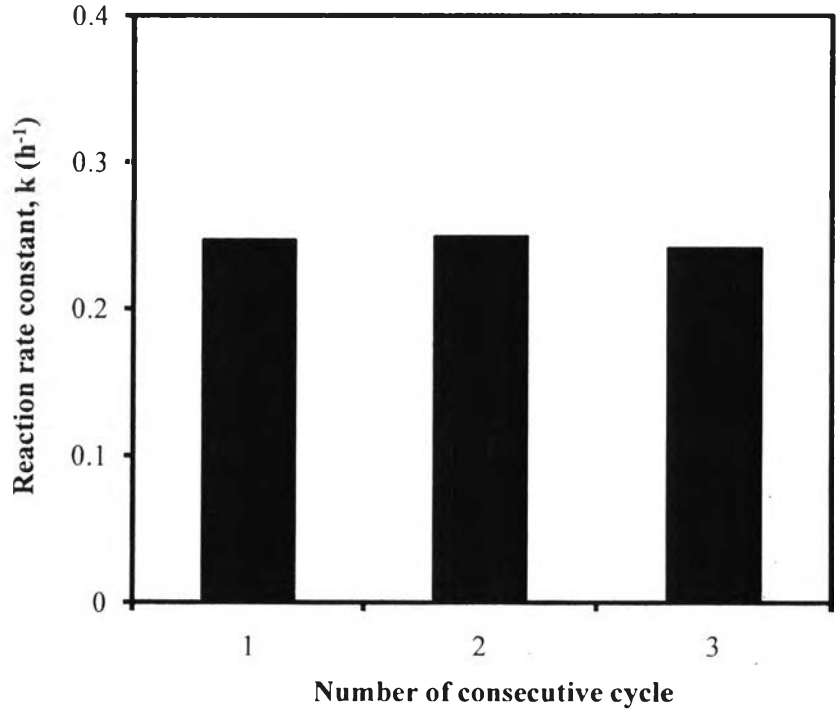

Figure 4.25 Effect of recyclability of the synthesized mesoporous-assembled TiO_2 photocatalyst film with 5 wt.% P-25 TiO_2 addition on reaction rate constant for AB dye degradation (total reaction mixture volume, 500 ml; initial AB dye concentration, 10 mg/l; initial solution pH, 5.04; calcination temperature, 400 °C; number of coated TiO_2 layer, 4 layer; number of TiO_2-coated glass plate, 8 plates; and irradiation time, 4 h).

4.2.8 Photocatalytic Activity Comparison between the Immobilized and Suspended Synthesized Mesoporous-Assembled TiO_2 Photocatalyst with 5 wt.% P-25 TiO_2 Addition

The powders of the synthesized mesoporous-assembled TiO_2 photocatalyst with 5 wt.% P-25 TiO_2 addition were obtained by scraping from the films initially coated on eight glass plates. The photocatalytic AB dye degradation activity of the powders was compared to that of the films (with identical quantity of TiO_2 photocatalyst). It was found that the utilization of TiO_2 photocatalyst in the suspension mode (powders) showed a greater photocatalytic activity as compared to the immobilization mode (films), as expected. The TiO_2 powders could completely degrade the AB dye within 1.5 h, whereas a longer time of more than 5 h was

required for the complete AB dye degradation in case of the TiO_2 films. This is plausibly due to the much higher accessibility of the AB dye and active species molecules to the available surface active sites in case of the TiO_2 powders.